

# Once-Training-All-Fine: No-Reference Point Cloud Quality Assessment via Domain-relevance Degradation Description

Yipeng Liu, Qi Yang, Yujie Zhang, Yiling Xu, Le Yang, Xiaozhong Xu, Shan Liu

**Abstract**—Full-reference (FR) point cloud quality assessment (PCQA) has achieved impressive progress in recent years. However, as reference point clouds are not available in many cases, no-reference (NR) metrics have become a research hotspot. Existing NR methods suffer from poor generalization performance. To address this shortcoming, we propose a novel NR-PCQA method, Point Cloud Quality Assessment via Domain-relevance Degradation Description ( $D^3$ -PCQA). First, we demonstrate our model’s interpretability by deriving the function of each module using a kernelized ridge regression model. Specifically, quality assessment can be characterized as a leap from the scattered perceptual domain (reflecting subjective perception) to the ordered quality domain (reflecting mean opinion score). Second, to reduce the significant domain discrepancy, we establish an intermediate domain, the description domain, based on insights from subjective experiments, by considering the domain relevance among samples located in the perception domain and learning a structured latent space. The anchor features derived from the learned latent space are generated as cross-domain auxiliary information to promote domain transformation. Furthermore, the newly established description domain decomposes the NR-PCQA problem into two relevant stages. These stages include a classification stage that gives the degradation descriptions to point clouds and a regression stage to determine the confidence degrees of descriptions, providing a semantic explanation for the predicted quality scores. Experimental results demonstrate that  $D^3$ -PCQA exhibits robust performance and outstanding generalization ability on several publicly available datasets. The code in this work will be publicly available at <https://smt.sjtu.edu.cn>.

**Index Terms**—Point cloud, blind quality assessment, subjective modeling, learning-based metric

## 1 INTRODUCTION

Recently, point cloud data has emerged as a promising representation format for representing 3D objects in various applications [1], [2]. A point cloud is a collection of non-uniformly scattered 3D points that may suffer from impairments in both geometry and attributes (e.g., color) during processing, resulting in perceptual degradation. To facilitate quality of experience (QoE)-oriented tasks (e.g., compression [3], [4] and enhancement [5], [6]), point cloud quality assessment (PCQA) has gained significant attention among researchers. PCQA can be achieved through subjective experiments or objective metrics. However, although subjective experiments can provide the ultimate prediction, they can be expensive in terms of time, cost and testing conditions [7]. Therefore, designing effective objective metrics has become a hotspot in recent research. Objective metrics can be categorized as full-reference (FR), reduced-reference (RR) and no-reference (NR) methods. FR and RR metrics

require the entire original samples or partial features as a reference, which may not be readily available in most scenarios. Thus, we focus on NR metrics as they are designed for scenarios where the high-quality original point cloud is not available.

### 1.1 Motivation

Current NR metrics are mostly based on deep learning. The common strategy is to use well-designed deep neural networks to map the input point clouds into the feature space, and then regress the final scores using the obtained latent features [8], which can be formulated as  $q = f(\phi(x))$ , where  $x$  and  $q$  represent the input point cloud and final objective score, and  $\phi(\cdot)$  and  $f(\cdot)$  represent the feature extraction and quality mapping operation. However, the performance of this architecture, especially in terms of generalization, is far from satisfactory. The main reason is that this paradigm ignores or weakens some important intermediate developments of subjective evaluation.

The process of quality assessment entails the transformation between different domains. Based on the study of the human visual system (HVS), we know that vision begins with the cone cells in the retina. The layer of nerve cells transmits visual signals to the brain, culminating in the generation of the final quality perception [9], [10]. We define the distribution of immediate visual stimuli of samples perceived by the HVS as the **perception domain**, and the distribution of final subjective quality scores as the **quality**

*This paper is supported in part by National Natural Science Foundation of China (61971282, U20A20185). The corresponding author is Yiling Xu (e-mail: yl.xu@sjtu.edu.cn).*

*Y. Liu, Y. Zhang and Y. Xu are from Cooperative Medianet Innovation Center, Shanghai Jiaotong University, Shanghai, 200240, China, (e-mail: liuyipeng@sjtu.edu.cn, yujie19981026@sjtu.edu.cn, yl.xu@sjtu.edu.cn)*

*Q. Yang, X. Xu, S. Liu are from Media Lab, Tencent, Shenzhen, China, (e-mail: chinoyang@tencent.com, xiaozhongxu@tencent.com, shanl@tencent.com)*

*L. Yang is from the Department of electrical and computer engineering, University of Canterbury, Christchurch 8041, New Zealand, (e-mail: le.yang@canterbury.ac.nz)*

*Corresponding author: Y. Xu*

**domain.** The perception domain has high dimensionality due to the presence of massive visual information, while the quality domain is a hierarchically ordered space with a limited range typically from 0-5 or 0-10 depending on the settings of the subjective experiment [11], [12]. The HVS does not acquire a straightforward mapping from the perception domain to the quality domain. Instead, it requires a training session before rating and the inherent experience to cultivate the prior knowledge, signifying the intrinsic relevance within each quality level [13], as auxiliary information to facilitate domain transformation. Subsequently, the individual viewer can foster a basic judgment regarding the degradation degree, which, however, is insufficient for accurately representing a testing sample in the quality domain due to personal limitations and biases. Therefore, current subjective experiments incorporate confidence correction to refine this basic judgment based on averaging scores obtained from multiple participants, leading to the establishment of mean opinion score (MOS).

Objective methods align with subjective perception in their shared objective of achieving domain transformation. However, NR-PCQA methods face a first problem stemming from the scattered distribution of training data in the perception domain, which hinders model fitting. Point clouds exhibit greater complexity in terms of geometry and attributes compared with images. Nevertheless, existing PCQA datasets, such as PointXR [14], IRPC [15], ICIP2020 [16], M-PCCD [17], SJTU-PCQA [12], and WPC [18], [19] typically consist of merely a few hundred distorted point clouds, resulting in only a few dozen samples for each distortion type. Considering the significant variability in content and distortion types, the available distorted point clouds are usually dispersedly scattered in the high-dimensional perception domain, resulting in a huge domain discrepancy with the ordered quality domain. The huge domain discrepancy poses challenges for domain transformation.

The second problem arises from the disparity between subjective experiments, which require a physiological mechanism, and the current NR-PCQA frameworks that attempt to establish a direct mapping relationship between the perception domain and the quality domain. The HVS prefers to generate discrete semantic descriptions for perceived quality based on the prior knowledge [20], [21], using integers to represent the perceived quality level as shown in Table 1, such as “5” to describe “the distortion is almost imperceptible”. However, the final MOSs are typically floating numbers that are the statistic results obtained from multiple participants, e.g., at least 16 reliable subjective scores are required to calculate the MOS [22]. The integral part of the MOS signifies the fundamental quality level, referring to the discrete semantic descriptions, whereas the decimal part can be interpreted as a confidence degree, which naturally establishes an intermediate domain between the perception domain and the quality domain.

We define this intermediate domain as the **description domain** which pertains to the feature distribution for discrete semantic descriptions. The clustering of perception domain features corresponding to quality-aware information gives rise to the generation of the description domain, and the elements in the quality domain serve as the fine-grained

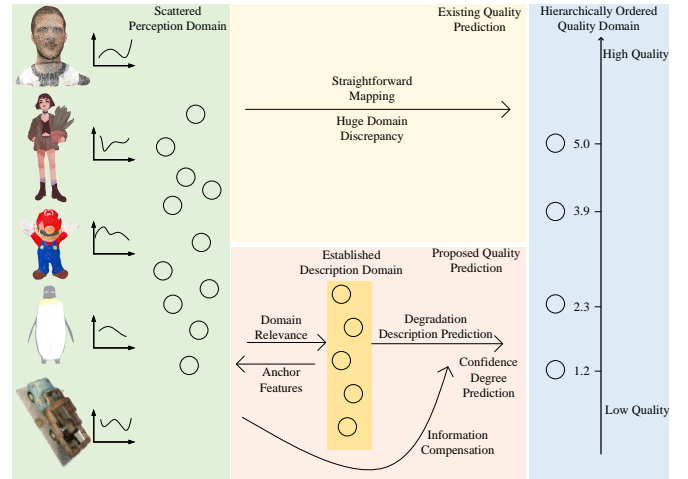


Fig. 1 Comparison between existing NR-PCQA methods and the proposed method. The huge discrepancy between the perception domain and the quality domain poses a challenge in establishing a reliable mapping. To address this issue, the proposed method introduces a new description domain by considering the relevance among samples located in the perception domain, which helps to narrow the domain discrepancy.

expression of the description domain features. However, most current objective methods neglect the expression of this description domain, resulting in neural networks needing to span a huge domain discrepancy and being more susceptible to content-aware information rather than quality-aware information, as shown in Fig. 1.

The third problem is that most NR-PCQA methods utilize a projection-based backbone which converts point clouds to images with predefined resolutions. This choice is made due to its lower memory usage and faster inference speed when compared with consuming 3D schemes [11]. However, these projection images exhibit different perceptions compared with original point clouds, primarily due to information loss and masked distortions, limiting the performance potential of projection-based methods.

## 1.2 Our Approach

We propose a novel NR-PCQA method called Point Cloud Quality Assessment via Domain-relevance Degradation Description ( $D^3$ -PCQA) regarding the above problems.  $D^3$ -PCQA establishes the ignored description domain which decomposes the quality prediction into two stages. For better explanation, we set the generation of quality level as Stage-1 and the generation of confidence degree as Stage-2.

First, to implement the proposed method, the training set is divided into a support set and a query set. The support set which is divided into five quality levels according to Table 1 is used to establish the description domain, and the query set is used to train the quality prediction network which will be introduced in the following part.

In Stage-1, we predict the quality level by learning a structured latent space, which reproduces the function of the description domain. We improve SCNN, a lightweight

neural network backbone, to generate the perception domain features with a HVS-based projection method which represents point clouds by emulating the effect of observation distance on HVS. To establish the description domain, the perception domain features are first disentangled into the domain-invariant features by a proposed Residual Transformer Network. Then the required structured latent space is learned by promoting the regular distribution of the disentangled features using the support set with a series of constraints. This process exploits the intrinsic relevance among different samples of the same quality level (namely intra-domain relevance). The clustering centers corresponding to each quality level, which contain the representative feature for the local description domain, can be used as the **anchor features** to promote domain transformation. Finally, we measure the relevance between the query set samples and the five anchor features (namely inter-domain relevance) and map it into the quality level by a proposed classification network.

In stage-2, we assess the confidence degree of the assigned quality level by measuring the feature relevance within the local description domain corresponding to a specific quality level. To do so, we utilize the perception domain features as information compensation. The measurement and mapping of feature relevance between the query set sample and the support set samples of determined quality level (which is yet another instance of intra-domain relevance) are approached as a regression problem, leading to the determination of the confidence degree. Finally, we obtain the final quality score by combining the quality level generated in Stage-1 with the confidence degree derived from Stage-2.

To elucidate the roles and functionalities of individual modules within the artificial neural network, we derive the pipeline of each module from a kernelized ridge regression model.

### 1.3 Contributions

The contributions of this paper are summarized as follows:

- We propose a novel NR-PCQA method called D<sup>3</sup>-PCQA to emulate the working mechanisms of subjective experiments.
- We greatly improve the generalization ability for quality prediction by exploiting the intra-domain relevance to establish the description domain.
- The proposed D<sup>3</sup>-PCQA shows reliable performance and outstanding generalization ability. Additionally, further experiments demonstrate the model’s scalability when integrated with 3D backbones.

The rest of this paper is organized as follows. The related work is surveyed in Section 2. Section 3 derives the function of each module from the solutions to a kernelized ridge regression problem. Section 4 presents the network implementation of the proposed D<sup>3</sup>-PCQA, with its performance evaluation given in Section 5. Finally, the conclusion is drawn in Section 6.

## 2 RELATED WORK

This section reviews existing PCQA metrics.

For FR-PCQA, Moving Picture Experts Group (MPEG) has applied point-to-point (p2point) [23], point-to-plane (p2plane) [24] and PSNRyuv [25] in point cloud compression (PCC) standardization. Other point-wise metrics, such as those proposed in [24], [26] and [27], have also been made available. Considering the geometry and color attributes simultaneously, Meynet *et al.* [28] proposed a metric that pools curvature statistics and color lightness together via optimally-weighted linear combination [29]. Viola *et al.* [30] suggested quantifying point cloud quality using color histograms. Alexiou *et al.* [31] incorporated four types of point cloud attributes into the form of SSIM [32]. Yang *et al.* [33] utilized color gradient to estimate point cloud quality based on graph signal processing. Zhang *et al.* [34] proposed a HVS-based multi-scale method that can be integrated into several PCQA metrics. Javaheri *et al.* [35] developed a point-to-distribution metric to measure point cloud quality.

Another approach for FR-PCQA is to project the 3D point cloud onto a number of 2D planes and then represent point cloud quality using the weighted indices of these image planes. Torliget *et al.* [36] proposed real-time voxelization and projection techniques to present point clouds and evaluated IQA metrics for PCQA. Alexiou *et al.* [26] measured the distortion using the angles between tangent planes perpendicular to point normals. Yang *et al.* [12] combined global and local features of projection planes to estimate point cloud quality. Javaheri *et al.* [37] proposed a joint geometry and color projection and applied 2D quality metrics to reflect point cloud quality.

For RR-PCQA, Viola *et al.* [38] inferred point cloud quality using statistical information of geometry, color and normal vector. Q. Liu *et al.* [39] and Y. Liu *et al.* [40] estimated quality using compression parameters to guide PCC strategy with certain rate constraints.

The above-mentioned PCQA metrics are categorized into FR and RR metrics, which necessitate both distorted point clouds and their reference versions as inputs. However, acquiring the reference version can be challenging in practical scenarios, prompting the development of NR metrics. Like in FR-PCQA, NR metrics can be performed either over the 2D projection of point clouds or directly on the raw data. For methods conducted over point cloud projection, Tao *et al.* [41] employed multi-scale feature fusion to predict the quality of point clouds. Liu *et al.* [42] proposed to leverage distortion classification information as an auxiliary feature to assist in the training of the network. Yang *et al.* [43] bridged conventional images and point cloud projection via domain adaptation to expand the scale of trainable point cloud data. Fan *et al.* [44] and Zhang *et al.* [45] integrated the point cloud projection into a video, followed by the utilization of video quality assessment methods for the purpose of evaluating the quality of point clouds. For methods over raw 3D data, Liu *et al.* [11] adopted an end-to-end sparse convolution network to learn the quality representation of point clouds. Shan *et al.* [46] extracted anti-perturbation features for point clouds using a graph neural network. In addition, other algorithms have been developed that leverage both point cloud projection and raw 3D data to extract integrated features, as exemplified by the work of Zhang *et al.* [47]. Most existing NR-PCQA methods adopt a uniform architecture of feature extraction using

a range of techniques, followed by regression into score values that fail to accurately emulate the intricate human visual mechanism. In this work, we aim to introduce a fresh approach to the NR-PCQA problem by mapping extracted features to align with human perception.

### 3 PROBLEM FORMULATION

In this section, we illustrate each module of D<sup>3</sup>-PCQA from the perspective of a kernelized ridge regression to better understand the architecture of the proposed method.

Given the training samples  $\{x_i, y_i\}_{i=1}^N$ , we can formulate NR-PCQA as a generalized linear ridge regression problem:

$$w = \arg \min_w \sum_{i=1}^N (y_i - w^T \phi(x_i))^2 + \frac{\lambda}{2} \|w\|^2, \quad (1)$$

where  $x_i$  is the  $i$ -th distorted sample,  $y_i$  is the *continuous* quality score,  $\phi(\cdot)$  represents the nonlinear feature mapping;  $N$  is the total number of training samples. Besides,  $w$  is the regression vector, and  $\lambda$  signifies the trade-off parameter for the regularization term. The solution to (1) is the weighted sum of the training samples (i.e.,  $w = \sum_{i=1}^N \alpha_i \phi(x_i)$ ), according to the well-known representer theorem [48].

In order to establish a new intermediate domain between the perception domain and the quality domain, we may express the label  $y$  and response  $r = w^T \phi(x)$  in (1) as the summation of an integer quality level and decimal degree of confidence. As a result, we can decompose the original NR-PCQA task aimed at producing a continuous objective score into the combination of a multi-class classification problem that finds the integer quality level corresponding to the degradation quantification and a regression problem that generates the degree of confidence. Mathematically, we have

$$y = y_L + y_R, \quad (2)$$

$$r = w^T \phi(x) = r_L + r_R, \quad (3)$$

where  $y_L$  and  $r_L$  indicate the *integer* quality level of  $y$  and  $r$ , and  $y_R$  and  $r_R$  represent the *decimal* degree of confidence of  $y$  and  $r$ .

#### 3.1 Stage-1: Semantic Degradation Description Prediction

The degradation description defined by BT.500 [22] (Table 1) of a testing sample  $x_i$  can be determined by classifying  $y_{i,L} \in \{1, 2, 3, 4, 5\}$ . In order to establish the description domain corresponding to  $y_{i,L}$ , the training samples are grouped according to the distribution of their normalized quality scores. Correspondingly, the summands in (1) can be organized in groups and the quality level can then be determined by concatenated ridge regression models:

$$w_L = \arg \min_{w_L} \sum_{j=1}^{N/K} \left[ \sum_{i=1}^K (y_{i,j,L} - w_{j,L}^T \phi(x_{i,j}))^2 + \frac{\lambda}{2} \|w_{j,L}\|^2 \right], \quad (4)$$

where  $x_{i,j}$  signifies the  $i$ -th samples in the  $j$ -th quality level group, and  $K$  is the number of training samples for each quality level.  $w_L$  is defined as  $w_L = \{w_{j,L}\}_{j=1}^{N/K}$ . Note that

TABLE 1 Five-grade degradation description defined by BT.500 [22].

MOS	Degradation Description
5	The distortion is almost imperceptible
4	The distortion is perceptible but not annoying
3	The distortion is slightly annoying
2	The distortion is annoying
1	The distortion is seriously annoying

in (4), the regressand has been changed to  $y_{i,j,L}$ , the class label corresponding to the degradation description of  $y_{i,j}$ . In other words, it is now a multi-class classification problem and we aim at identifying the sample's quality level (in terms of  $y_{i,j,L} \in \{1, 2, 3, 4, 5\}$ ). The regression vector for the  $j$ -th quality level is, again from the representer theorem [48],

$$w_{j,L} = \sum_{i=1}^K \alpha_{i,j,L} \phi(x_{i,j}). \quad (5)$$

Here,  $x_{i,j}$  is the  $i$ -th distorted sample with its quality level equal to  $j$ . Using (5) transforms (4) into

$$\alpha_L = \arg \min_{\alpha_L} \sum_{j=1}^{N/K} \left[ \sum_{i=1}^K (y_{i,j,L} - \sum_{k=1}^K \alpha_{k,j,L} \phi^T(x_{k,j}) \phi(x_{i,j}))^2 + \frac{\lambda}{2} \sum_{i=1, k=1}^K \alpha_{i,j,L} \alpha_{k,j,L} \phi^T(x_{k,j}) \phi(x_{i,j}) \right]. \quad (6)$$

Let  $k(x_{k,j}, x_{i,j}) = \phi^T(x_{k,j}) \phi(x_{i,j})$  be the positive definite kernel function. As a result, for sample  $x_{i,j}$ , the response under a particular quality level  $j$  would be

$$r_{i,j,L} = \sum_{k=1}^K \alpha_{k,j,L} k(x_{k,j}, x_{i,j}) = \sum_{k=1}^K \alpha_{k,j,L} \phi^T(x_{k,j}) \phi(x_{i,j}). \quad (7)$$

In other words,  $w_{j,L} = \sum_{k=1}^K \alpha_{k,j,L} \phi(x_{k,j})$  can be considered as the common feature extracted from the samples with the  $j$ -th quality level, which can characterize a representative feature for the local description domain corresponding to a specific degradation description. Let

$$\phi_j(x_m) = w_{j,L} = \sum_{k=1}^K \alpha_{k,j,L} \phi(x_{k,j}). \quad (8)$$

We call  $\phi_j(x_m)$  the **anchor feature** deriving from the intra-domain relevance of a specific quality level.

The response in (7) can be rewritten as

$$r_{i,j,L} = \phi_j^T(x_m) \phi(x_{i,j}) = k_j(x_m, x_i). \quad (9)$$

The kernel function  $k_j(x_m, x_i)$  now measures the inter-domain relevance between an input distorted sample  $x_i$  and the anchor feature  $\phi_j(x_m)$  for  $j$ -th quality level. Therefore, we indeed utilize the relevance measurement to classify the degradation description for quality assessment.

The kernel function  $k_j(x_m, x_i)$  in (9) may be evaluated using the following quadratic form to further take into

account the interaction between elements in the feature vectors  $\phi_j(x_m)$  and  $\phi(x_{i,j})$ :

$$k'_{m,i,j} = \phi_j^T(x_m)\beta_{j,L}\phi(x_{i,j}), \quad (10)$$

as long as the trainable matrix  $\beta_{j,L}$  is at least positive semidefinite. In the alternating iteration method, the method in [49] can be invoked to approximate the estimated  $\beta_{j,L}$  using the nearest (in terms of Frobenius norm  $\|\cdot\|_F$ ) positive semidefinite matrix.

Substituting (10) into (6), we obtain the following optimization problem

$$\begin{aligned} \alpha_L, \beta_L = \arg \min_{\alpha_L, \beta_L} & \sum_{j=1}^{N/K} \left[ \sum_{i=1}^K (y_{i,j,L} - \phi_j^T(x_m)\beta_{j,L}\phi(x_{i,j}))^2 \right. \\ & \left. + \frac{\lambda_1}{2} \sum_{i=1, k=1}^K \alpha_{i,j,L} \alpha_{k,j,L} k'_{i,k,j} + \frac{\lambda_2}{2} \|\beta_{j,L}\|_F^2 \right]. \end{aligned} \quad (11)$$

The solution to (11) can be obtained by leveraging the anchor feature through evaluating  $\phi_j(x_m) = \sum_{k=1}^K \alpha_{k,j,L} \phi(x_{k,j})$ ,  $j = 1, 2, \dots, 5$ . For an unseen distorted sample  $x_i$ , its degradation description can then be determined using  $r_{i,j,L} = \phi_j^T(x_m)\beta_{j,L}\phi(x_i)$ . The value of  $j$  corresponding to the largest  $r_{i,j,L}$  would be output as the quality level of  $x_i$ .

### 3.2 Stage-2: Confidence Degree Prediction

We can adopt the same nonlinear ridge regression framework in (11) to map the coarse-grained quality level obtained in Stage-1 into the accurate quality score in the quality domain. Specifically, with slight abuse of notations, we aim at solving

$$\begin{aligned} \alpha_R, \beta_R = \arg \min_{\alpha_R, \beta_R} & \sum_{j=1}^{N/K} \left[ \sum_{i=1}^K (y_{i,j,R} - \sum_{k=1}^K \alpha_{k,j,R} \phi^T(x_{k,j})\beta_{j,R}\phi(x_{i,j}))^2 \right. \\ & \left. + \frac{\lambda_1}{2} \sum_{i=1, k=1}^K \alpha_{i,j,R} \alpha_{k,j,R} k'_{i,k,j} + \frac{\lambda_2}{2} \|\beta_{j,R}\|_F^2 \right]. \end{aligned} \quad (12)$$

The regressand  $y_{i,j,L}$ , which is the class label for quality level prediction, is replaced with  $y_{i,j,R}$ , which is the decimal degree of confidence. Note that the main difference is that the anchor feature  $\phi_j(x_m)$  for  $j$ -th quality level is not calculated first. Instead, the entire formula is employed to measure the intra-domain relevance between  $\phi(x_{i,j})$  and sample features of a specific quality level. This is because measuring feature relevance is critical for fine-tuning.

Since here both  $\alpha_R$  and  $\beta_{j,R}$  contribute to mapping the relevance,  $\beta_{j,R}$  in (12) is fixed to be identity matrix of an appropriate size to reduce the computational burden. We thus only need to find  $\alpha_R$  such that the estimated decimal degree of confidence for an unseen sample  $x_i$ , whose quality level was found to be equal to  $j$ , can be calculated using  $\sum_{k=1}^K \alpha_{k,j,R} \phi^T(x_{k,j})\phi(x_i)$ . Combining this result with the obtained quality level yields the final estimate of the continuous quality score for a testing sample.

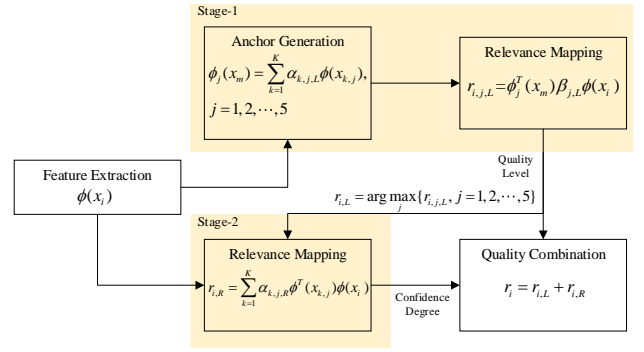


Fig. 2 Functions of derived modules. The derivation decomposes the conventional regression-based architecture into 2 relevant stages by establishing a new description domain, with the domain relevance being utilized for both domain establishment and domain transformation.

### 3.3 Functions of Derived Modules

Based on the above derivation, several modules can be identified from the response terms of (11) and (12), as illustrated in Fig. 2. The proposed method includes the following modules:

- **Feature Extraction:** The original feature of sample  $x_i$  is extracted from a feature extraction backbone, denoted as  $\phi(x_i)$ .
- **Anchor Feature Generation:** The description domain is established, where the *anchor feature* for  $j$ -th quality level is generated by measuring the *intra-domain relevance* among sample features in the perception domain, which is  $\phi_j(x_m) = \sum_{k=1}^K \alpha_{k,j,L} \phi(x_{k,j})$ ,  $j = 1, 2, \dots, 5$ .
- **Relevance Mapping:** In Stage-1, the quality level is determined by measuring the *inter-domain relevance* between the sample feature and five anchor features, i.e.,  $r_{i,L} = \arg \max_j \{ \phi_j^T(x_m)\beta_{j,L}\phi(x_i), j = 1, 2, \dots, 5 \}$ . In Stage-2, the confidence degree is determined by measuring the *intra-domain relevance* among samples of the determined quality level, which is  $r_{i,R} = \sum_{k=1}^K \alpha_{k,j,R} \phi^T(x_{k,j})\phi(x_i)$ .
- **Quality Combination:** The quality level and the confidence degree are combined to generate the continuous quality score, given as  $r_i = r_{i,L} + r_{i,R}$ .

## 4 NETWORK IMPLEMENTATION

We implement the equivalent functions for the response terms of (11) and (12) using neural networks. The proposed D<sup>3</sup>-PCQA aims at expressing the ignored description domain for performance improvement, whose overall architecture is depicted in Fig. 3. The proposed framework consists of several modules, including the feature extraction module (symbolized as  $\phi(\cdot)$ ), the anchor feature generation module, the relevance mapping module (denoted as  $G(\cdot)$  and  $H(\cdot)$ ) and the quality combination module. Among them, the

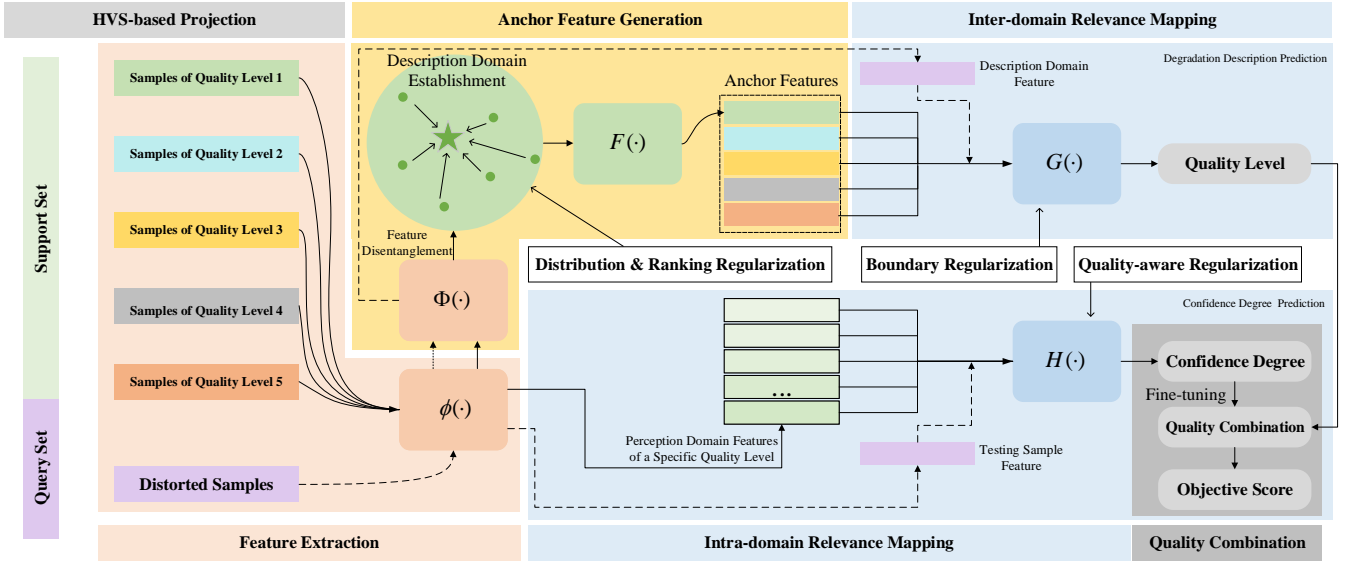


Fig. 3 Overall architecture of  $D^3$ -PCQA.  $D^3$ -PCQA is divided into 2 stages: degradation description prediction and confidence degree prediction. To implement  $D^3$ -PCQA, the training samples are partitioned into the support set and the query set, and the support set is further partitioned into five-grade impairment scales based on BT.500 [22]. In Stage-1, the feature extraction module  $\phi(\cdot)$  extracts the perception domain features, using the HVS-based projection, which are disentangled using the feature disentanglement module  $\Phi(\cdot)$ . The description domain is established with a series of constraints based on the disentangled features in the support set, and then the anchor feature for each quality level is generated using the feature aggregation module  $F(\cdot)$ . The relevance mapping module  $G(\cdot)$  solves the degradation description prediction as a classification problem by measuring the inter-domain relevance between the query set samples and five anchor features. In Stage-2, the relevance mapping module  $H(\cdot)$  regresses the confidence degree based on the intra-domain relevance within the local description domain corresponding to the determined quality level. The quality combination module finally combines the quality level and the confidence degree to obtain the continuous quality score.

anchor feature generation module involves the feature disentanglement (represented by  $\Phi(\cdot)$ ), the description domain establishment, and the feature aggregation (indicated by  $F(\cdot)$ ). In the following subsections, we will detail each of these modules.

To implement the proposed method, inspired by [50], [51], the training samples are partitioned into a support set and a query set. We use the support set to establish the description domain and to generate the anchor features. Then, we train the quality prediction network using the query set.

We illustrate the transformation between different domains of the output of each module in Fig. 4. The feature extraction module  $\phi(\cdot)$  extracts the scattered perception domain features that reflect the visual stimuli. The feature disentanglement module  $\Phi(\cdot)$  extracts the description domain-related components from the perception domain features, and then the anchor feature generation using  $F(\cdot)$  and the quality level prediction using  $G(\cdot)$  can be performed in the description domain which is established with a series of constraints. Finally, leveraging the perception domain features,  $H(\cdot)$  predicts the confidence degree for generating the elements in the quality domain, i.e., the continuous quality scores.

The network implementation also takes into account the functions of the regularization terms in (11) and (12). The regularization term which is intended to reduce overfitting is achieved through weight decay during network training.

Meanwhile, the regularization term for ensuring that the kernel matrix is positive semidefinite, thereby guaranteeing that the output is nonnegative, is accomplished through the use of imposed activation functions.

To provide better illustration, we use the established description domain to decompose our proposed model into two stages, i.e., Stage-1 to predict the quality level and Stage-2 to generate the confidence degree. Note that although we have staged our demonstration for clarity, our proposed method is an **end-to-end** framework, and the two stages mutually reinforce each other.

#### 4.1 Feature Extraction Module

The proposed  $D^3$ -PCQA architecture is versatile and not limited to either 2D or 3D features. In this work, we focus on the projection-based backbone to extract the perception domain features, which consumes less memory and has a faster inference speed compared with the 3D-based schemes. Besides, in Section 5.8, we also test 3D-based backbones to demonstrate the generalization ability and scalability of our method. In this subsection, we introduce some important visual characteristics to improve the 2D backbone to obtain projection images that are consistent with human perception for feature extraction.

##### 4.1.1 Simulation of HVS Observation Mechanism

The information loss in immediate point cloud projection derives from the mismatch between the point cloud size

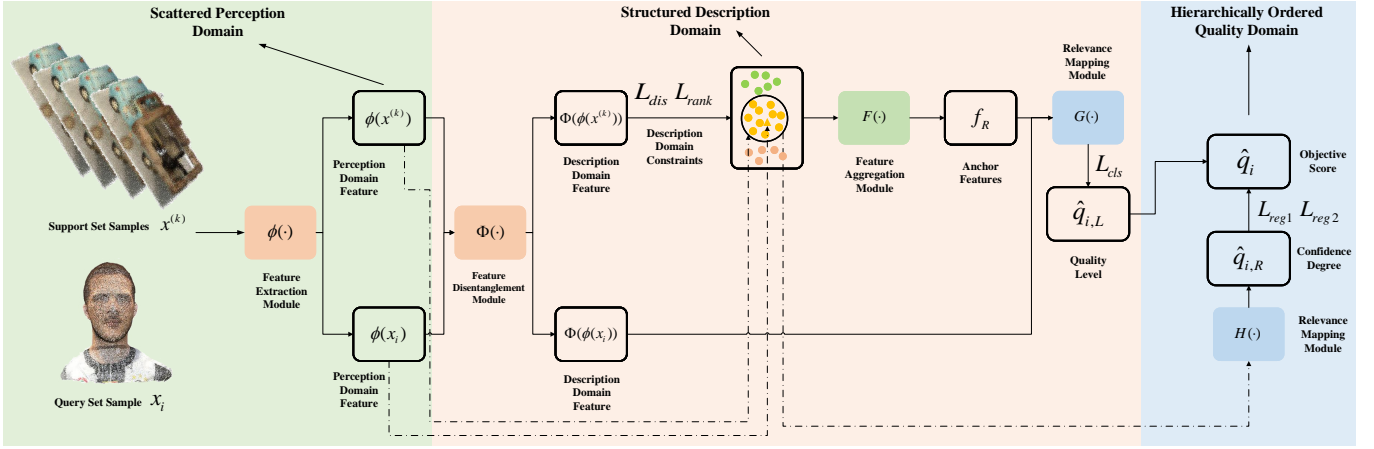


Fig. 4 Transformation between different domains of the output of each module. The module symbols and parameter variables are consistent with those in Fig. 3 and in Section 4.  $\phi(\cdot)$  extracts the scattered perception domain features.  $\Phi(\cdot)$  extracts the description domain-related components from the perception domain features, and then the anchor feature generation using  $F(\cdot)$  and the quality level prediction using  $G(\cdot)$  can be performed in the description domain which is established with the constraints  $\mathcal{L}_{dis}$  and  $\mathcal{L}_{rank}$ . Finally, leveraging the perception domain features,  $H(\cdot)$  predicts the confidence degree for generating the elements in the quality domain, i.e., the continuous quality scores.

and projection plane size. Additionally, 2D encoders usually require regular-size input images, which are typically much smaller than the point cloud size for mini-batch training. Existing methods, such as the cropping method in [41] and the folding method in [52], have been used to maintain consistent input sizes across samples, but they distort the whole perception and introduce extra distortions. To address these issues, our work calls upon the HVS-based multi-scale representation of point clouds.

Specifically, projecting one point cloud onto one small viewing window can be simulated as how human eyes perceive distant point clouds. As the viewing distance increases, our perception is affected by several visual phenomena, i.e., scale reduction, loss of detail and blurring. These factors contribute to the construction of point cloud presentation at different scales. According to [34], point clouds with a relatively small scale, resulting from long observation distances, still match well with subjective scores. Based on this, reducing the original point clouds to a small scale based on the HVS mechanism can contribute to the generation of projection images with a regular and small size.

By simulating the above three visual phenomena when human eyes observe point clouds from a distance, a new 2D representation of point clouds is established. The generation process of this new 2D representation consists of three steps, i.e., region rescaling, projection and low-pass filtering.

**Region Rescaling.** In order to map the point cloud  $P = [P^C, P^O] \in R^{N \times 6}$  onto the 2D plane  $Z$ , all points of the point cloud are initially moved towards the center of the bounding box until matching the size of the projection images, thereby simulating the size change with increased viewing distance. We define this operation as region rescaling, denoted as  $\Psi(\cdot)$ . The geometry attribute  $P^C$  of  $P$  is modified, while the color attribute  $P^O$  remains unchanged. The resulting point cloud can be represented by

$$P_1 = [\Psi(P^C), P^O] \in R^{N \times 6}. \quad (13)$$

To ensure that the points of the point cloud and the pixels of the projection image align, the points are converted to voxels by rounding the coordinates. The resulting point cloud can be signified as

$$P_2 = [\Gamma(\Psi(P^C)), P^O] \in R^{N \times 6}, \quad (14)$$

where  $\Gamma$  is the round-off operation which leads to the blurring in geometrical coordinates.

In this process, the point density  $\rho$  of the point cloud will be changed, which is defined as the number of points per unit volume. Specifically, for a local patch  $P_s$  located within the corresponding sphere region  $N(s, R_s)$ , the point density can be calculated as

$$\rho = \frac{|P_s|}{\frac{4}{3}\pi R_s^3}. \quad (15)$$

Given the bounding box size of the point cloud,  $[[X_{min}, X_{max}], [Y_{min}, Y_{max}], [Z_{min}, Z_{max}]]$ , and the projection image size,  $[[x_{min}, x_{max}], [y_{min}, y_{max}]]$ , we can calculate the scaling factor, symbolized as  $\delta$ , using the equation

$$\delta = \frac{\min(|\Delta x|, |\Delta y|)}{\max(|\Delta X|, |\Delta Y|, |\Delta Z|)}, \quad (16)$$

where  $|\Delta x| = x_{max} - x_{min}$ , and  $\Delta x$  and  $\Delta y$  are usually the same. The point density of the resulting point cloud can be denoted as

$$\rho' = \frac{|P_s|}{\frac{4}{3}\pi(\delta \cdot R_s)^3}. \quad (17)$$

**Projection.** The point cloud  $P_2$  is mapped orthographically onto a pre-determined 2D plane  $Z$  to generate a texture projection image  $I_1 \in N^{W \times H \times 3}$  and a depth projection image  $I_2 \in N^{W \times H \times 3}$  where  $W = x_{max} - x_{min}$  and  $H = y_{max} - y_{min}$ . Each pixel  $i^1$  in  $I_1$  is filled by the color attribute of the corresponding point in the point cloud, while each pixel  $i^2$  in  $I_2$  is filled by the geometry attribute of the corresponding point in the point cloud. Due

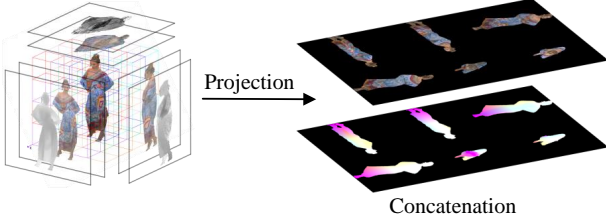


Fig. 5 Texture and depth projection. Six RGB texture maps and six depth maps are generated for each point cloud. Then six perspectives are spliced together into a multi-perspective image.

to the scaling down of the point cloud during the projection process, some points corresponding to the same pixel are discarded, resulting in loss of detail. Then inspired by [43], we splice together six different perspectives to generate a multi-perspective image to address the uneven information density across different perspectives, as illustrated in Fig. 5.

**Low-pass Filtering.** To further simulate the color blurring as the scale decreases, the blurring operation is applied to the projection images. To introduce the additional blurring distortion, we use a low-pass filtering operation defined as  $f(\cdot)$ . The texture projection image  $I_1$  is filtered into  $I'_1$ , while the depth projection image  $I_2$  is filtered into  $I'_2$ . The filtered projection image can be represented by

$$I'_1 = f(I_1) \in N^{W \times H \times 3}, \quad (18)$$

and

$$I'_2 = f(I_2) \in N^{W \times H \times 3}. \quad (19)$$

The low-pass filter can be implemented by averaging the neighborhood  $N(x, R)$  within a certain radius of  $R$  which varies linearly with the change in point density:

$$f(x) = \frac{1}{|N(x, R)|} \sum_{i \in N(x, R)} x_i \quad (20)$$

$$\text{s.t. } R = \begin{cases} k(\tau - \rho'), & \text{if } \rho' < \tau \\ 0, & \text{if } \rho' \geq \tau \end{cases},$$

where  $\tau$  is an empirical critical point density for the watertight surface, which represents the threshold at which the change in point density will not affect subjective perception.

When the point clouds are normalized into a consistent scale and the sphere region  $N(s, R_s)$  is sufficiently large to encompass the complete point cloud, the radius  $R$  can be approximated as

$$R = \begin{cases} k(\tau - \rho'), & \text{if } \rho' < \tau \\ 0, & \text{if } \rho' \geq \tau \end{cases} \\ = \begin{cases} k\left(\frac{|P_\tau|}{\frac{4}{3}\pi R_s^3} - \frac{|P'|}{\frac{4}{3}\pi R_s^3}\right), & \text{if } \frac{|P'|}{\frac{4}{3}\pi R_s^3} < \frac{|P_\tau|}{\frac{4}{3}\pi R_s^3} \\ 0, & \text{if } \frac{|P'|}{\frac{4}{3}\pi R_s^3} \geq \frac{|P_\tau|}{\frac{4}{3}\pi R_s^3} \end{cases} \quad (21) \\ = \begin{cases} k'(|P_\tau| - |P'|), & \text{if } |P'| < |P_\tau| \\ 0, & \text{if } |P'| \geq |P_\tau| \end{cases}.$$

In other words, the degree of introduced blurring can be determined by the change in point number caused by the distortions.

When  $|P'| < |P_\tau|$ , (21) can be rewritten as

$$R = k'(|P_\tau| - |P'|) = k'|P_\tau|\left(1 - \frac{|P'|}{|P_\tau|}\right) = R_m\left(1 - \frac{|P'|}{|P_\tau|}\right), \quad (22)$$

where  $R_m$  indicates the filter radius corresponding to the blurring distortion.

#### 4.1.2 Subjective Experiment

We conduct a compact subjective experiment to demonstrate the validity of the proposed HVS-based point cloud projection. Specifically, the point clouds with down-sampling distortion are selected from the SJTU-PCQA [12] dataset for the subjective experiment. These distorted point clouds are projected onto planes of size  $224 \times 224$  from six perspectives using two projection methods. The first method involves an immediate projection without any additional operations, while the second method involves three steps mentioned in Sec 4.1.1. The resulting six-perspective projection images are spliced together to generate a multi-perspective image for the subjective experiment [43]. To evaluate the projection quality, these projection images are mixed and shuffled and then evaluated by human viewers using the subjective experiment process as defined in BT.500 [22].

The results of the correlation performance are presented in Table 2, which is calculated based on the scores obtained from the subjective experiment and the ground truth MOS. Additionally, defining the scoring error as the absolute difference between the obtained score and MOS, a statistical analysis of the scoring errors is conducted, and the results are shown in Table 3. The scale of the obtained scores and MOS ranges from 1-10. According to Table 2 and Table 3, it is evident that the proposed HVS-based projection shows better correlation with the subjective perception compared with the immediate projection.

TABLE 2 Correlation performance between the subjective scores and ground truth MOS for the immediate projection and the proposed projection.

	Immediate Projection	HVS-based Projection
PLCC	0.73	0.92
SROCC	0.59	0.88

TABLE 3 Mean, standard deviation and 95% quantile of the scoring errors for two projection schemes.

	Immediate Projection	HVS-based Projection
Mean	2.3543	1.1189
Standard Deviation	1.6135	0.8278
95% Quantile	5.1331	2.7552

#### 4.1.3 Backbone

After performing the HVS-based projection for point clouds, we utilize a backbone (denoted as  $\phi(\cdot)$ ) to extract the raw features of these projections. These raw features can represent the immediate visual stimuli perceived by the HVS. We call them the perception domain features. Although the



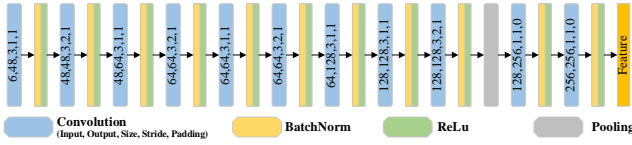


Fig. 6 Feature extraction backbone for D<sup>3</sup>-PCQA.

feature extraction backbone is not the main focus of this paper, it is required to be lightweight and extract robust features for PCQA. Following the work in [43], we propose a modified lightweight network based on [53], as shown in Fig 6. Each convolutional layer in Fig 6 is characterized by the input channel, output channel, kernel size, stride and padding, and is followed by batch normalization and a nonlinearity activation function (ReLU).

## 4.2 Anchor Feature Generation Module

Referring to (8), the anchor features can be considered the common features for a specific quality to facilitate the domain transformation and can be extracted from a weighted combination of sample features that share the same degradation description, denoted as

$$\phi_j(x_m) = \sum_{k=1}^K \alpha_{k,j} \phi(x_{k,j}) = W_\alpha \phi_j(x^{(k)}), \quad (23)$$

where  $j$  signifies the  $j$ -th quality level,  $K$  is the size of a mini-batch,  $\phi_j(x^{(k)}) \in R^{K \times d_f}$  represents the sample features of the  $j$ -th quality level, and  $d_f$  is the feature dimension.

This operation requires extracting common characteristics but cannot handle the scattered distribution in the perception domain features. Therefore, in the network implementation, we first disentangle the perception domain features using a proposed Residual Transformer Network into the domain-invariant features. Then a structured latent space is learned to establish the description domain by regularizing the distribution of the disentangled features. Finally, a series of anchor features can be aggregated from the learned structured latent space to drive domain transformation for quality level prediction.

To learn the anchor features, we assume that the samples in the support set follow a uniform distribution across various impairment scales, and we divide the support set into 5 groups corresponding to five-grade degradation descriptions [22] based on their MOS.

### 4.2.1 Feature Disentanglement

The attainment of anchor features necessitates the structured distribution within a learned latent space which reproduces the function of the description domain. However, directly restricting the distribution of the perception domain feature  $\phi(x^{(k)})$ , which is extracted from the backbone, may not yield the desired results. As explained earlier,  $\phi(x^{(k)})$  represents the differentiated stimuli perceived by the HVS and scatters in the perception domain. Thus, we propose a Residual Transformer Network to disentangle the perception domain features into the domain-invariant features and

the domain-specific features. The domain-invariant features which capture the cross-sample common characteristics for a specific quality level are utilized for description domain establishment.

**Domain-invariant Feature Disentanglement.** The perception domain feature  $\phi(x^{(k)})$  is considered to contain two components, i.e., the domain-invariant features that are shared among samples located in the local description domain corresponding to the same quality level, and the domain-specific features related to the specific manifestation from different source domains. The former exists based on the common characteristics of the same quality level. The latter, such as the specific texture information of the sample itself, is responsible for the huge discrepancy among samples in the perception domain. Hence, the domain-invariant features are first extracted before regularizing the feature distribution to learn the structured latent space.

To fully consider the interaction between samples, inspired by [54], we employ a Residual Transformer [55] Network to combine features. This module projects  $f_p^{(k)} = \phi(x^{(k)}) \in R^{K \times d_f}$  into queries  $Q \in R^{K \times d}$ , keys  $K \in R^{K \times d}$  and values  $V \in R^{K \times d}$  using linear projections, where  $Q = \phi(x^{(k)})W_q$ ,  $K = \phi(x^{(k)})W_k$ , and  $V = \phi(x^{(k)})W_v$ . To compute the weighted sum of the values  $v$  as the combined output, the scaled dot-product is applied to obtain the cross-sample attention weight:

$$\alpha_A = \text{softmax}\left(\frac{QK^T}{\sqrt{d}}\right), \quad (24)$$

which generates the similarity weight based on  $K$  and  $Q$ . The weighted feature as output is given by

$$\begin{aligned} Y &= \alpha_A V - \frac{1}{K} [1] \phi(x^{(k)}) \\ &= \alpha_A \phi(x^{(k)}) W_v - \frac{1}{K} [1] \phi(x^{(k)}) \\ &\approx \left(\alpha_A - \frac{1}{K} [1]\right) \phi(x^{(k)}), \end{aligned} \quad (25)$$

where  $[1]$  signifies the matrix with all elements equal to 1, and  $K$  is the length of the mini-batch.  $\phi$  and  $W_v$  both map the single features, leading to the approximate ignorance of  $W_v$  [54], and (25) achieves the interaction between different features required by (23).

The proposed Residual Transformer Network can extract the domain-invariant features across samples by measuring the similarity between  $f_p$  and other features in the mini-batch, thus leveraging the intra-domain relevance among samples with the same quality level. Additionally, during training, the shuffle operation has been implemented to introduce dynamic mini-batches, thereby diminishing the reliance of output features on specific content of individual samples as the training progresses.

**Module Structure.** This module denoted as  $\Phi(\cdot)$  can be

formulated as

$$\begin{aligned}
y_0 &= [\phi(x^{(1)}), \phi(x^{(2)}), \dots, \phi(x^{(K)})], \\
Q_i &= K_i = V_i = \text{FC}(y_{i-1}), \\
y'_i &= \text{MSA}(Q_i, K_i, V_i), \\
y_i &= \text{FFN}(y'_i), \quad i = 1, \dots, l, \\
[f_{E_1}, f_{E_2}, \dots, f_{E_K}] &= y_l - \text{mean}(y_0), \\
f_E &= [f_{E_1}, f_{E_2}, \dots, f_{E_K}],
\end{aligned} \tag{26}$$

where  $y_0$  represents the input mini-batch containing  $K$  extracted perception domain features of the same quality level,  $f_E = \Phi(\phi(x^{(k)}))$  gives the output domain-invariant features, and  $l$  is the number of layers which equals 2 in this work. FC means the fully connected layer, and FFN means the feed-forward network [55], which corresponds to the feature mapping in (25). MSA signifies the multi-head self-attention module [55] which refers to the feature interaction in (24) and (25).

#### 4.2.2 Description Domain Establishment

Since each quality level shares the same degradation description, there exists intra-domain relevance among samples within the same quality level. Therefore, we make an assumption that the extracted domain-invariant features for different quality levels can exhibit a structured distribution in a latent space. Such a structured latent space is learned in the support set by imposing a series of constraints to reproduce the function of the description domain, which is crucial for improving the generalization ability.

**Distribution Regularization.** We expect the disentangled features from the same quality level to cluster together in the latent space as they refer to the same abstract semantic characteristics. For instance, features of score 5 represent ‘‘imperceptible distortion’’, and features of score 1 represent ‘‘seriously annoying distortion’’. Conversely, the features from different quality levels should be mutually exclusive. To enforce this, we use a normalized temperature-scaled cross-entropy loss [56] to restrict the distribution of disentangled features, i.e.,

$$\mathcal{L}_{dis} = \frac{1}{K} \sum_{i=1}^K \frac{1}{|P(i)|} \sum_{j \in P(i)} -\log \frac{\exp(\text{sim}(f_i, f_j) / \tau)}{\sum_{k=1}^K \mathbf{1}_{k \neq i} \exp(\text{sim}(f_i, f_k) / \tau)}, \tag{27}$$

where  $f_i = \Phi(\phi(x_i))$  represents the extracted domain-invariant features,  $\text{sim}(f_i, f_j) = f_i^T f_j / \|f_i\|_2 \|f_j\|_2$  is to measure the similarity between  $f_i$  and  $f_j$ ,  $K$  is the number of point clouds in the mini-batch,  $\mathbf{1}$  is the indicator function,  $\tau$  is the temperature parameter,  $P(i)$  is a set containing point cloud indices belonging to the same quality level as  $y_i$  (but excluding the index  $i$ ) and  $|P(i)|$  is its cardinality.

By imposing the distribution regularization, the disentangled features that are causally associated with the degradation description can be regularly distributed in the learned latent space.

**Structured Ranking Regularization.** To further regularize the learning of the latent space, we utilize the rank information among different samples. In quality assessment, accurate ranking has greater importance than precise classification. For example, a point cloud with a score of 2.6 can be classified into either level 2 or level 3, but it is important to place it between samples with scores of 2 and 3. The ranking performance can

be measured by Spearman rank order correlation coefficient (SROCC), which is defined as follows:

$$\text{SROCC}(q, \hat{q}) = 1 - \frac{6 \sum_{i=1}^L (m_i - n_i)^2}{L(L^2 - 1)}, \tag{28}$$

where  $q$  is the true MOS,  $\hat{q}$  is the predicted quality score,  $L$  is the number of distorted point clouds,  $m_i$  is the rank of  $q_i$  in the MOS, and  $n_i$  is the rank of  $\hat{q}_i$  in the predicted quality scores. SROCC can also be computed from Pearson linear correlation coefficient (PLCC):

$$\text{SROCC}(q, \hat{q}) = \text{PLCC}(R(q), R(\hat{q})), \tag{29}$$

where  $R$  represents the rank function, which is defined as

$$R(x) = \sum_{x_i \in x^{(k)}} H(x - x_i) \tag{30}$$

where  $H(x)$  is the Heaviside step function. And PLCC is defined as

$$\text{PLCC}(q, \hat{q}) = \frac{\sum_{i=1}^L (q_i - q_m)(\hat{q}_i - \hat{q}_m)}{\sqrt{\sum_{i=1}^L (q_i - q_m)^2} \sqrt{\sum_{i=1}^L (\hat{q}_i - \hat{q}_m)^2}}, \tag{31}$$

where  $q_m$  and  $\hat{q}_m$  are the arithmetic mean of MOS  $q$  and predicted scores  $\hat{q}$ . When given a mini-batch and transforming (31) into the loss function:

$$\text{loss}_{plcc} = \frac{\sum_{k=1}^K (q_k - q_m)(\hat{q}_k - \hat{q}_m)}{\sqrt{\sum_{k=1}^K (q_k - q_m)^2} \sqrt{\sum_{k=1}^K (\hat{q}_k - \hat{q}_m)^2}}, \tag{32}$$

where  $K$  is the length of the mini-batch. Then the structured ranking loss can be denoted as

$$\begin{aligned}
\mathcal{L}_{rank} &= -\text{loss}_{srocc}(q^{(k)}, \hat{q}_L^{(k)}) \\
&= -\text{loss}_{plcc}(R(q^{(k)}), R(\hat{q}_L^{(k)})),
\end{aligned} \tag{33}$$

where  $\hat{q}_L^{(k)}$  gives the predicted quality levels across the mini-batch.  $q^{(k)}$  indicates the ground truth MOS.  $R$  represents the rank function. Existing methods such as [42] have utilized PLCC as the loss function, because  $\text{loss}_{plcc}$  is derivable. However, the required  $\text{loss}_{srocc}$  is not derivable due to the existence of the Heaviside step function. We utilize a constrained linear program, inspired by Google Research’s Fastsorting [57], to approximate the rank function in (33), denoted as

$$R_{\varepsilon Q}(x) = P_{\varepsilon Q}(-x, \rho) = P_Q(-x/\varepsilon, \rho) \tag{34}$$

$$P_Q(z, w) = \underset{\mu \in \mathcal{P}(w)}{\text{argmax}} \langle z, \mu \rangle - Q(\mu) = \underset{\mu \in \mathcal{P}(w)}{\text{argmin}} \frac{1}{2} \|\mu - z\|^2 \tag{35}$$

where  $\rho = (n, n-1, \dots, 1)$ .  $\underset{\mu \in \mathcal{P}(w)}{\text{argmax}} \langle z, \mu \rangle$  is the linear program, and  $Q(\mu) = \frac{1}{2} \|\mu\|^2$  is quadratic regularization.  $\mathcal{P}(w) = \text{conv}(\{w_\sigma : \sigma \in \Sigma\}) \subset \mathbb{R}^n$  represents the convex hull of permutations of  $w$ .

### 4.2.3 Feature Aggregation

After enforcing the learned latent space to exhibit a structured distribution, the clustering center characterizes the local description domain corresponding to a specific quality level and can serve as an anchor feature to distinguish different quality levels. These anchor features provide auxiliary information beyond the perception domain, thereby helping sample features achieve domain transformation more easily.

To generate the anchor feature, the regularized domain-invariant features from samples of the same quality level are aggregated to further reduce dependence on sample characteristics. This module denoted as  $F(\cdot)$  can be formulated as

$$f_R = \frac{1}{K} \sum_k \Phi(\phi(x^{(k)})) \approx \frac{1}{K} e(\underbrace{\alpha_A - \frac{1}{K}[1]}_{W'_\alpha}) \phi(x^{(k)}), \quad (36)$$

where  $e$  is the unit vector.  $f_R$  is the obtained anchor feature for a specific quality level. (36) which exhibits a similar formulaic expression to that of (23) illustrates that the network implemented for generating the anchor features aggregates the common features for a specific quality level.

## 4.3 Relevance Mapping Module for Stage-1

### 4.3.1 Inter-domain Relevance Mapping

Referring to the response term in (11), the inter-domain relevance between the testing sample feature and five anchor features is measured and then mapped into the quality level, denoted as

$$r_{i,L} = \arg \max_j \{\phi_j^T(x_m) \beta_{j,L} \phi(x_i), j = 1, 2, \dots, 5\}, \quad (37)$$

where the relevance is measured through element-wise multiplication and is mapped using the matrix  $\beta_{j,L}$  in the alternating iteration method. However, this mapping operation, denoted as  $F_1(A, B) = (A \odot B) \times W_1$  where  $\odot$  represents the element-wise multiplication, only maps the relevant results and cannot make full use of the entire information from the samples and the description domain. In contrast, we use a network to perform both functions: relevance measurement and relevance mapping.

To make full use of the anchor features derived from the support set, we concatenate them with the testing sample features from the query set. This compensates the sample feature with the information in the description domain. Subsequently, we use a mapping network to measure the inter-domain relevance between the testing sample and five anchor features and mapped it into the probability scores of each quality level that the testing samples belong to. The quality levels of testing samples can be determined by the one with maximum. In fact, we demonstrate that the proposed network operation denotes as  $F_2(A, B) = [A; B] \times W_2$  is a special case of the operation  $F_1$  in (37) (i.e. **Theorem 1**).

**Theorem 1.** For  $F_1(A, B) = (A \odot B) \times W_1$ ,  $F_2(A, B) = [A; B] \times W_2$ , if  $W_1 = [W_2./B, W_2./A]$ ,  $F_1 = F_2^T$ .

*Proof.* Substituting  $W_1 = [W_2./B, W_2./A]$  into  $F_2(A, B) = [A; B] \times W_2$ , we obtain the following formula:

$$\begin{aligned} F_2(A, B) &= [A; B] \times W_2 \\ &= [A \times W_2; B \times W_2] \\ &= ([A \odot B] \times [W_2./B, W_2./A])^T \\ &= ([A \odot B] \times W_1)^T \\ &= F_1^T(A, B) \end{aligned}$$

□

**Theorem 1** explains that the output of the operation  $F_2$  in the proposed network, represented by  $F_2(A, B) = [A; B] \times W_2$ ,

can be expressed as the output of the operation in (37), denoted as  $F_1(A, B) = (A \odot B) \times W_1$ , with a special weight matrix  $W_1$ . This proves that  $F_2$  is a special case of  $F_1$ .

**Module Structure.** This module denoted as  $G(\cdot)$  can be formulated as

$$\begin{aligned} g_s &= \text{cat}([f_{x_i} \oplus f_{R,j}, j = 1, \dots, 5]), \\ g_1 &= FC(256 \times 2 \times 5, 64)(g_s), \\ g_2 &= \text{Relu}(g_1), \\ g_3 &= FC(64, 5)(g_2), \\ g_c &= \text{argmax}(\text{Softmax}(g_3)), \end{aligned} \quad (38)$$

where  $g_c$  is the output of  $G$  identified as the predicted quality level,  $f_{x_i} = \Phi(\phi(x_i))$  in which the sample  $x_i$  from the query set is mapped into the learned latent space to prevent additional errors due to offsets in the feature space,  $f_{R,j}$  gives the anchor feature for the  $j$ -th quality level, and  $\text{cat}$  and  $\oplus$  represent the concatenation operation. FC means the fully-connected layers which are characterized by the input and output channel number.

The forward propagation for Stage-1 can be represented as

$$\hat{q}_{i,L} = G(F(\Phi(\phi(x^{(k)}))), \Phi(\phi(x_i))), \quad (39)$$

where  $x^{(k)}$  signifies the support set samples,  $x_i$  denotes the testing sample in the query set, and  $\hat{q}_{i,L}$  is the predicted quality level.

### 4.3.2 Boundary Regularization

We use the ground truth quality level of the testing sample in the query set to constrain the training of the networks involved in Stage-1. This ensures that the networks are trained with correct quality level information. Additionally, the objective function for classification can promote the learning of bounded features for different quality levels in the latent space. To train the network for 5-class classification, the following cross entropy loss is adopted:

$$L_{cls} = \frac{1}{K} \sum_{i=1}^K \sum_{j=1}^5 -q_{i,j,L} \log \hat{q}_{i,j,L} - (1 - q_{i,j,L}) \log (1 - \hat{q}_{i,j,L}), \quad (40)$$

where  $\hat{q}_{i,j,L}$  gives the predicted quality level,  $q_{i,j,L}$  represents the ground truth quality level, and  $K$  is the length of the mini-batch.

By applying the boundary regularization, the clustering centers in the learned latent space connect with the optimization objectives, i.e., the quality levels. This promotes the development of distinctions between features with different quality levels in the learned latent space.

## 4.4 Relevance Mapping Module for Stage-2

### 4.4.1 Intra-domain Relevance Mapping

Referring to the response term in (12), the intra-domain relevance between the testing sample in the query set and the samples of the same  $j$ -th quality level in the support set is measured to obtain the confidence degree using

$$r_{i,R} = \sum_{k=1}^K \alpha_{k,j,R} \phi^T(x_{k,j}) \phi(x_i), \quad (41)$$

which quantifies the relevance between the sample  $x_i$  and other samples around  $x_i$  within the local description domain.

The domain-invariant features extracted in the previous subsection are designed specifically for the description domain. Besides, the disentangled features can cause information loss, which can limit the quality prediction from the description domain to the quality domain. Therefore, in this stage, we leverage the perception domain features  $\phi(x)$  to measure the



(a) tool\_box gQP:26 cQP:26  
MOS: 85  
Score: 3.9

(b) tool\_box gQP:44 cQP:32  
MOS: 71  
Score: 3.7

(c) ship gQP:44 cQP:38  
MOS: 41  
Score: 3.2

(d) ship gQP:50 cQP:50  
MOS: 27  
Score: 2.1

Semantics: The distortion is perceptible but not annoying

Semantics: The distortion is perceptible but not annoying

Semantics: The distortion is slightly annoying

Semantics: The distortion is annoying

Fig. 7 Exemplary point clouds with the subjective MOS, the predicted quality score of the proposed D<sup>3</sup>-PCQA and the semantic degradation description corresponding to the predicted quality level on the WPC dataset. The predicted quality score and the semantic degradation description align with subjective perception.

relevance of neighboring points in the description domain. Similar to the operation in the previous subsection, we measure and map the relevance using the concatenated features by a mapping network. In this way, the network can perceive the feature components related to the quality difference, and the quality domain can be connected with a smaller discrepancy.

**Module Structure.** This module denoted as  $H(\cdot)$  is formulated as

$$\begin{aligned} h_s &= \phi_{x_i} \oplus \phi_{x_j}^{(k)}, \\ h_k &= FC(256 \times 2, 64)(h_s^{(k)}), \\ h_k &= Relu(h_k), \\ h_k &= FC(64, 1)(h_k), \\ h_k &= Sigmoid(h_k) - 0.5, \quad k = 1, \dots, K, \\ h_r &= mean([h_1, h_2, \dots, h_K]), \end{aligned} \quad (42)$$

where  $h_r$  gives the output of  $H$  identified as the predicted confidence degree,  $\phi_{x_i} = \phi(x_i)$  represents the extracted perception domain features of the sample  $x_i$  in the query set,  $\phi_{x_j}^{(k)} = \phi(x_j^{(k)})$  indicates the extracted perception domain features of samples in the support set identified as the  $j$ -th quality level by Stage-1, and  $K$  is the sample number for the  $j$ -th quality level in the mini-batch.

The forward propagation for Stage-2 is

$$\hat{q}_{i,R} = H(\phi(x^{(k)}), \phi(x_i)), \quad (43)$$

where  $x^{(k)}$  signifies the support set samples,  $x_i$  is the testing sample in the query set, and  $\hat{q}_{i,R}$  represents the predicted confidence degree.

#### 4.4.2 Quality-aware Regularization

We use the PLCC loss and SROCC loss defined above as loss functions to explicitly improve them, i.e.,

$$\mathcal{L}_{reg1} = -loss_{plcc}(\hat{q}^{(k)}, q^{(k)}), \quad (44)$$

and

$$\mathcal{L}_{reg2} = -loss_{srocc}(\hat{q}^{(k)}, q^{(k)}). \quad (45)$$

Here,  $\hat{q}^{(k)} = \hat{q}_L^{(k)} + \hat{q}_R^{(k)}$  is the predicted continuous quality scores across a mini-batch which is the sum of the quality levels and the confidence degree values.  $q^{(k)}$  gives the ground truth MOS.

Besides, the modules involved in Stage-1 operate on the extracted domain-invariant features. The imposed quality-aware regularization can ensure that the quality-aware common components exist in the original features.

## 4.5 Cross-stage Training Mechanism

The two stages of the proposed architecture are not independent and mutually reinforce each other. Stage-1 serves as the foundation for Stage-2, and Stage-2, in turn, facilitates the establishment of the latent space in Stage-1. Specifically, when the network is inadequately trained and predicts the quality level inaccurately, the quality-aware regularization seeks to achieve a large value of  $\hat{H}(x)$  which separates the feature  $\phi(x)$  of the testing sample from those of “similar” samples determined in Stage-1. Essentially, it increases the differences between mismatched samples. Conversely, under accurate quality level prediction,  $H(x)$  facilitates the feature differences based on the quality differences, promoting a structured distribution in the learned latent space.

## 4.6 Quality Combination Module

Given the support set samples  $x^{(k)}$ , the continuous quality score of the sample  $x_i$  in the query set can be obtained by

$$\begin{aligned} \hat{q}_i &= \hat{q}_{i,L} + \hat{q}_{i,R} \\ &= G(F(\Phi(\phi(x^{(k)}))), \Phi(\phi(x_i))) + H(\phi(x^{(k)}), \phi(x_i)), \end{aligned} \quad (46)$$

where  $\hat{q}_i$  is the desired predicted continuous quality score.

## 4.7 Overall Loss

The overall training loss is the sum of distribution loss, structured ranking loss, boundary loss and two quality-aware losses, which leads to

$$\mathcal{L} = \mathcal{L}_{dis} + \mathcal{L}_{rank} + \mathcal{L}_{cls} + \mathcal{L}_{reg1} + \mathcal{L}_{reg2}. \quad (47)$$

# 5 EXPERIMENTAL RESULTS AND ANALYSES

## 5.1 Datasets

To evaluate the performance of the proposed D<sup>3</sup>-PCQA, we conduct evaluation experiments on three independent datasets, i.e., LS-PCQA [11], SJTU-PCQA [12] and WPC datasets [18], [19].

**LS-PCQA.** The LS-PCQA [11] dataset consists of 104 reference point clouds with 31 different types of distortions under 7 levels. These distortions include geometry distortions, attribute distortions and compression distortions, resulting in a total of 22,568 distorted point cloud samples.

**SJTU-PCQA.** The SJTU-PCQA [12] dataset consists of 9 reference point clouds with 7 different types of distortions under 6 levels. These distortions comprise 4 individual distortions and 3 superimposed distortions, resulting in a total of 378 distorted point cloud samples.

**WPC.** The WPC [18], [19] dataset consists of 16 reference point cloud samples with V-PCC distortion, considering the combination between 5 geometry quantization steps and 5 texture quantization steps, resulting in a total of 400 distorted samples.

To compare the proposed D<sup>3</sup>-PCQA with other learning-based NR-PCQA metrics, we split the LS-PCQA, SJTU-PCQA and WPC datasets into the training sets and the testing sets. The training set and the testing set from LS-PCQA contain the distorted samples generated from 100 and 4 reference point clouds respectively to avoid overlapping. For SJTU-PCQA and WPC, we split the reference point clouds of the two datasets such that 75% of the samples are used for training, while the remaining 25% are for testing.

To augment the training sets, for projection-based methods, each point cloud is projected to 12 versions of images by rotating it to 12 different viewpoints. The 12 viewpoints are uniformly placed around the object based on the 12 polyhedron vertices of a regular icosahedron [42], [58]. For 3D-based methods, random rotation within the range of  $[0^\circ, 360^\circ)$  is invoked during training.

## 5.2 Overall Performance

The correlation metrics (PLCC and SROCC) are used to quantify the performance of the objective methods. We compare the performance of proposed D<sup>3</sup>-PCQA with prevalent FR metrics, including MSE-PSNR-P2point (M-p2po) [23], Hausdorff-PSNR-P2point (H-p2po) [23], MSE-PSNR-P2plane (M-p2pl) [59], Hausdorff-PSNR-P2plane (H-p2pl) [59], PSNRyuv [25], Hausdorff-PSNRyuv (H-PSNRyuv) [25], PCQM [29], GraphSIM [33] and MPED [60], prevalent 3D-based NR methods, including ResSCNN [11], GPA-Net [46] and MM-PCQA [47], and prevalent projection-based NR methods, including PQA-Net [42] and IT-PCQA [43]. Additionally, to evaluate the average performance of these methods across multiple datasets, we present the weighted mean values of PLCC and SROCC based on the scale of the testing sets. The results are summarized in Table 4, with the best results highlighted in bold and the second-best results highlighted with underline.

We can see from Table 4 that: i) the proposed D<sup>3</sup>-PCQA exhibits robust and outstanding performance across all three datasets. In contrast, the performance of existing FR and NR methods varies significantly across different datasets. For example, the proposed D<sup>3</sup>-PCQA achieves an SROCC of approximately 0.8 on all three datasets. Conversely, GPA-Net performs well on the SJTU-PCQA dataset with an SROCC of 0.87 but poorly on the LS-PCQA and WPC dataset with an SROCC of 0.60; ii) the proposed D<sup>3</sup>-PCQA improves the model fitting in the presence of huge domain discrepancy in the training data, leading to outstanding performance on the LS-PCQA and WPC datasets. For example, on LS-PCQA, a dataset with large domain discrepancy, the proposed D<sup>3</sup>-PCQA exhibits a high SROCC over 0.7, while other NR methods yield inferior performance with an SROCC below 0.6. Additionally, the proposed D<sup>3</sup>-PCQA achieves the best performance among the projection-based methods, albeit slightly inferior to 3D-based methods, on the less complex SJTU-PCQA dataset where 3D-based backbones offer greater advantages in utilizing the training data; iii) the performance of the proposed D<sup>3</sup>-PCQA can approach or even exceed that of existing FR metrics. For example, when comparing the (PLCC, SROCC) values of D<sup>3</sup>-PCQA and the FR metrics with the best performance on the three datasets, we obtain (0.75, 0.75) for D<sup>3</sup>-PCQA vs. (0.63, 0.62) for PSNRyuv on LS-PCQA, (0.80, 0.82) for D<sup>3</sup>-PCQA vs. (0.91, 0.89) for GraphSIM and MPED on SJTU-PCQA, and (0.81, 0.79) for D<sup>3</sup>-PCQA vs. (0.74, 0.75) for PCQM and GraphSIM on WPC.

While some NR methods may exhibit better performance than FR metrics, this does not necessarily mean that these NR methods are “superior”, but rather that they have better fitting performance. Therefore, we further evaluate the generalization performance of D<sup>3</sup>-PCQA and existing NR-PCQA methods in the following subsection.

Additionally, we show some examples of distorted point clouds with the subjective MOS, the predicted quality score of the proposed D<sup>3</sup>-PCQA and the semantic degradation description corresponding to the predicted quality level in Fig. 7. It can be observed that the predicted quality score and the semantic degradation description align with subjective perception.

## 5.3 Generalization Performance

In practice scenarios, the generalization ability assumes heightened significance. In this subsection, we evaluate the generalization ability of the proposed D<sup>3</sup>-PCQA through the cross-dataset experiment. Specifically, we consider two testing conditions: training on a small-scale dataset and testing on a small-scale dataset, and training on a large-scale dataset and testing on a small-scale dataset. In the first testing condition, the proposed D<sup>3</sup>-PCQA and other NR-PCQA methods are trained on the SJTU-PCQA dataset and tested on the WPC dataset. Then the two datasets are switched and the experiment is repeated. In the second testing condition, the proposed D<sup>3</sup>-PCQA and other NR-PCQA methods are trained on the LS-PCQA dataset and tested on the SJTU-PCQA and WPC datasets, respectively. The cross-dataset evaluation results are shown in Table 5. The best results are highlighted in bold, and the second-best results are highlighted with underline.

We can see from Table 5 that: i) the proposed D<sup>3</sup>-PCQA exhibits superior generalization ability compared with other NR-PCQA methods under all testing conditions, highlighting its effectiveness. The SROCC achieved by the proposed D<sup>3</sup>-PCQA surpasses the second-best result under all testing conditions by approximately 0.2. Conversely, most existing learning-based NR methods exhibit unsatisfactory generalization ability. For example, in the first testing condition, the proposed D<sup>3</sup>-PCQA exhibits an SROCC of 0.7, while other NR-PCQA methods exhibit an SROCC of only approximately 0.5; ii) the utilization of the training data significantly affects the generalization performance of NR-PCQA models. In general, 3D-based NR-PCQA methods outperform projection-based methods, which is explained by the high efficiency in utilizing the training data of 3D-based backbones. However, in this case, the performance of the proposed D<sup>3</sup>-PCQA, despite using a projection-based backbone, still demonstrates superior generalization performance, showcasing the effectiveness of our method; iii) the coverage of the training data also affects the generalization performance of NR-PCQA models. Methods trained on the large-scale datasets benefit from training data with broader coverage, leading to higher generalization ability.

## 5.4 Performance Compared with Regression-based Architecture

The existing NR methods typically have a similar architecture. Generally, these methods extract features from raw point cloud data and then map these features into quality scores. In this subsection, we compare the overall performance and generalization performance between the proposed D<sup>3</sup>-PCQA with the conventional regression-based architecture. Specifically, the regression-based architecture can be achieved by  $G(\phi(x^{(k)}))$  where  $\phi$  represents the feature extraction backbone and  $G$  signifies the regression network.  $\phi$  and  $G$  of the testing network are kept identical to those in this paper. The results are shown in Table 6.

TABLE 4 Overall performance on the LS-PCQA, SJTU-PCQA and WPC datasets. The best results are highlighted in bold, while the second-best results are underlined. Modal P means that the methods operate on the raw 3D data, and Modal I indicates that the methods operate on the point cloud projection.

Type	Method	Modal	LS-PCQA		SJTU-PCQA		WPC		Weighted	
			PLCC	SROCC	PLCC	SROCC	PLCC	SROCC	PLCC	SROCC
FR	M-p2po	P	0.61	0.30	0.88	0.78	0.61	0.58	0.63	0.36
	M-p2pl	P	0.59	0.29	0.77	0.63	0.63	0.59	0.61	0.35
	H-p2po	P	0.52	0.26	0.60	0.58	0.51	0.46	0.53	0.30
	H-p2pl	P	0.53	0.26	0.65	0.62	0.55	0.48	0.54	0.31
	PSNRyuv	P	<u>0.63</u>	<u>0.62</u>	0.65	0.62	0.46	0.47	0.62	0.61
	H-PSNRyuv	P	0.60	<u>0.57</u>	0.43	0.41	0.29	0.23	0.56	0.52
	PCQM	P	0.40	0.54	0.84	0.83	0.74	0.75	0.47	0.58
	GraphSIM	P	0.43	0.46	<b>0.91</b>	<b>0.89</b>	0.74	0.75	0.50	0.52
	MPEd	P	0.44	0.40	<b>0.91</b>	<b>0.89</b>	0.65	0.61	0.50	0.46
NR	ResSCNN	P	0.60	<u>0.62</u>	0.86	0.81	0.72	0.75	0.63	<u>0.65</u>
	GPA-Net	P	<u>0.63</u>	0.60	<u>0.87</u>	<u>0.87</u>	0.58	0.60	<u>0.64</u>	0.62
	MM-PCQA	P+I	-	-	0.86	0.84	<u>0.77</u>	<u>0.77</u>	-	-
	PQA-Net	I	0.56	0.52	0.70	0.68	0.25	0.21	0.54	0.50
	IT-PCQA	I	0.51	0.53	0.58	0.63	0.55	0.54	0.52	0.54
	D <sup>3</sup> -PCQA (ours)	I	<b>0.75</b>	<b>0.75</b>	0.80	0.82	<b>0.81</b>	<b>0.79</b>	<b>0.76</b>	<b>0.76</b>

TABLE 5 Generalization performance of NR-PCQA methods. The best results are highlighted in bold, while the second-best results are underlined. The proposed D<sup>3</sup>-PCQA exhibits the highest generalization ability under all testing conditions.

		ResSCNN		GPA-Net		MM-PCQA		PQA-Net		IT-PCQA		D <sup>3</sup> -PCQA (ours)	
Training	Testing	PLCC	SROCC	PLCC	SROCC	PLCC	SROCC	PLCC	SROCC	PLCC	SROCC	PLCC	SROCC
SJTU-PCQA	WPC	0.24	0.27	0.32	0.29	<u>0.48</u>	<u>0.41</u>	0.31	0.27	0.43	0.40	<b>0.64</b>	<b>0.60</b>
WPC	SJTU-PCQA	0.57	0.54	0.39	0.38	<u>0.70</u>	<u>0.62</u>	0.41	0.39	0.47	0.50	<b>0.76</b>	<b>0.70</b>
LS-PCQA	SJTU-PCQA	0.62	0.63	0.54	0.51	-	-	0.55	0.53	<u>0.71</u>	<u>0.64</u>	<b>0.85</b>	<b>0.85</b>
LS-PCQA	WPC	<u>0.53</u>	<u>0.53</u>	0.40	0.37	-	-	0.49	0.46	0.50	0.49	<b>0.75</b>	<b>0.73</b>

TABLE 6 Performance compared with the conventional regression-based architecture on the SJTU-PCQA and WPC datasets. The proposed D<sup>3</sup>-PCQA significantly improves the overall performance and generalization capability compared with the conventional regression-based architecture.

		Training	Testing	PLCC	Gain	SROCC	Gain
Single-dataset	Regression-based	SJTU-PCQA	SJTU-PCQA	0.71		0.70	
		WPC	WPC	0.68		0.67	
	Ours	SJTU-PCQA	SJTU-PCQA	<b>0.80</b>	↑ 12.68%	<b>0.82</b>	↑ 17.14%
		WPC	WPC	<b>0.81</b>	↑ 19.12%	<b>0.79</b>	↑ 17.91%
Cross-dataset	Regression-based	SJTU-PCQA	WPC	0.43		0.40	
		WPC	SJTU-PCQA	0.57		0.51	
	Ours	SJTU-PCQA	WPC	<b>0.64</b>	↑ 48.84%	<b>0.60</b>	↑ 50.00%
		WPC	SJTU-PCQA	<b>0.76</b>	↑ 33.33%	<b>0.70</b>	↑ 37.25%

We can see from Table 6 that: i) the proposed D<sup>3</sup>-PCQA outperforms the conventional regression-based architecture under both the single-dataset testing condition and the cross-dataset testing condition. This demonstrates the effectiveness of our proposed method in quality prediction; ii) the proposed D<sup>3</sup>-PCQA has a greater gain in the cross-dataset evaluation. This is explained by the effective strategy of exploring domain relevance in improving generalization ability.

## 5.5 Effect of Loss Functions

The proposed network is trained using the distribution loss, the structured ranking loss, the boundary loss and the two quality-aware losses. In this subsection, we evaluate the effect of each loss function on the WPC dataset. We use  $\mathcal{L}_{cls}$  to train the network as a benchmark. To demonstrate the effectiveness of establishing the description domain,  $\mathcal{L}_{cls} + \mathcal{L}_{dis}$  and  $\mathcal{L}_{cls} + \mathcal{L}_{dis} + \mathcal{L}_{rank}$  are used as the loss function to repeat the trial, as the distribution loss and the structured ranking loss are highly related to the formation of structured latent space. To demonstrate the effectiveness of the cross-stage training mechanism,  $\mathcal{L}_{cls} + \mathcal{L}_{dis} + \mathcal{L}_{rank} + \mathcal{L}_{reg}$  is used as the loss function to train the network, which achieves the final performance of the proposed model. The overall performance and cross-dataset performance are shown in Table 7 and Table 8, respectively.

TABLE 7 Overall performance with different loss functions on the WPC dataset.

$\mathcal{L}_{cls}$	$\mathcal{L}_{dis}$	$\mathcal{L}_{rank}$	$\mathcal{L}_{reg}$	PLCC	SROCC
✓	×	×	×	0.51	0.44
✓	✓	×	×	0.50	0.51
✓	✓	✓	×	0.60	0.58
✓	✓	✓	✓	0.81	0.79

TABLE 8 Generalization performance with different loss functions trained on the WPC dataset and tested on the SJTU-PCQA dataset.

$\mathcal{L}_{cls}$	$\mathcal{L}_{dis}$	$\mathcal{L}_{rank}$	$\mathcal{L}_{reg}$	PLCC	SROCC
✓	×	×	×	0.28	0.31
✓	✓	×	×	0.52	0.50
✓	✓	✓	×	0.70	0.64
✓	✓	✓	✓	0.76	0.70

We can see from Table 7 and Table 8 that: i) the sole use of  $\mathcal{L}_{cls}$  leads to poor performance. For point clouds with similar impairment degrees, a few distortion levels may not suffice to accurately describe their ranking relationship, thus reducing the correlation performance; ii)  $\mathcal{L}_{dis}$  and  $\mathcal{L}_{rank}$  significantly

improve the generalization ability for quality prediction by exploiting the intra-domain relevance within different samples and establishing the proposed structured latent space to reproduce the function of the description domain; iii)  $\mathcal{L}_{reg}$  leads to obvious gain in performance, which demonstrates that  $\mathcal{L}_{reg}$  can promote the learning of the structured latent feature space and quality-aware features, and the proposed cross-stage training mechanism is effective for improving the performance of the model.

## 5.6 Effect of Projection Strategies

In this work, we propose two methods to address the issue of information loss caused by the projection operation, i.e., the depth projection and the HVS-based projection. First, in addition to the texture projection, the proposed method in this work incorporates an extra depth projection image to enhance the projection of the point cloud. Second, we introduce a new representation at a small scale, which aligns with the way human eyes observe point clouds from a distance, to handle information loss. In this subsection, we conduct evaluation experiments to demonstrate the effectiveness of these two methods. Specifically, the network using only the texture projection and the network without the HVS-based projection are trained and tested under the same condition as the original network. The performance comparison is shown in Table 9.

TABLE 9 Effectiveness of two methods to handle information loss on the SJTU-PCQA dataset.

	PLCC	SROCC
Network without depth projection	0.74	0.71
Network without HVS-based projection	0.79	0.74
Proposed network	0.80	0.82

We can see from Table 9 that both proposed methods to handle information loss exhibit improvements in performance. The proposed depth projection enhances the utilization of training samples, while the HVS-based projection allows the model to respond to the masked distortions from a different perspective, thus enhancing the quality prediction capability of the model.

## 5.7 Selection of Maximum Blurring Degree

In the proposed feature extraction module, we adopt the blurring distortion as a substitute for the distortions masked by projection. To determine the maximum filter radius or blurring degree, denoted as  $R_m$ , we need to carefully choose an appropriate value. If  $R_m$  is set too small, the degree of blurring will not be enough to replace the masked distortions. Conversely, if  $R_m$  is set too large, the degree of blurring will not match the masked distortions, which will result in a discontinuity in the predicted quality scores. To determine the appropriate value for  $R_m$ , we conduct experiments in this subsection with the same setups as in Section 5.2 but with different  $R_m$  values. The overall performance and cross-dataset performance are shown in Table 10 and Table 11 respectively.

TABLE 10 Overall performance on the SJTU-PCQA dataset with different  $R_m$ .

$R_m$	PLCC	SROCC
5	0.79	0.78
10	0.80	0.82
15	0.82	0.77
20	0.73	0.72

We can see from Table 10 and Table 11 that  $R_m = 10$  is the most appropriate setting which exhibits the best overall performance and generalization ability.

TABLE 11 Generalization performance trained on the SJTU-PCQA dataset and tested on the WPC dataset with different  $R_m$ .

$R_m$	PLCC	SROCC
5	0.55	0.54
10	0.64	0.60
15	0.60	0.60
20	0.46	0.47

## 5.8 Scalability Demonstration

The proposed D<sup>3</sup>-PCQA is a versatile framework. While this paper mainly focuses on the projection-based NR-PCQA methods, the proposed framework is modular and can be integrated with other backbones. In this subsection, we utilize the proposed framework in conjunction with other backbones to illustrate its effectiveness and scalability. Specifically, we replace the 2D backbone in the proposed framework with the 3D backbones (ResSCNN and PointNet). To accelerate training, the 3D point clouds are downsampled to 1% of the original point number for the ResSCNN backbone and to 2,500 points for the PointNet backbone. The results of the experiments are shown in Table 12 and Table 13.

TABLE 12 Performance of the proposed D<sup>3</sup>-PCQA integrated with 3D backbones (1%-point sampling) on the SJTU-PCQA dataset.

	SJTU-PCQA			
	PLCC	Gain	SROCC	Gain
ResSCNN	0.66		0.67	
D <sup>3</sup> -PCQA + ResSCNN	0.91	↑ 37.88%	0.89	↑ 32.84%
PointNet	0.46		0.44	
D <sup>3</sup> -PCQA + PointNet	0.55	↑ 19.57%	0.56	↑ 27.27%

TABLE 13 Performance of the proposed D<sup>3</sup>-PCQA integrated with 3D backbones (1%-point sampling) on the WPC dataset.

	WPC			
	PLCC	Gain	SROCC	Gain
ResSCNN	0.45		0.43	
D <sup>3</sup> -PCQA + ResSCNN	0.50	↑ 11.11%	0.52	↑ 20.93%
PointNet	0.23		0.28	
D <sup>3</sup> -PCQA + PointNet	0.41	↑ 78.26%	0.49	↑ 75.00%

We can see from Table 12 and Table 13 that the proposed D<sup>3</sup>-PCQA is demonstrated to be effective in improving the performance for both 3D and 2D backbones, highlighting its generalization and scalability.

## 6 CONCLUSION

In this study, we propose a novel NR-PCQA method called D<sup>3</sup>-PCQA, which considers quality assessment as a domain transformation from the perception domain to the quality domain. To reduce domain discrepancy, we establish a new intermediate domain, namely the description domain, by exploiting domain relevance and learning a structured latent space. The anchor features derived from the learned structured latent space are generated as cross-domain auxiliary information to promote domain transformation. Furthermore, the established description domain decomposes quality prediction into the degradation description prediction and the confidence degree prediction, providing a semantic explanation for the predicted quality scores. Experimental results demonstrate the effectiveness of D<sup>3</sup>-PCQA, which achieves robust overall performance and outstanding generalization ability compared with existing NR-PCQA methods.

## REFERENCES

- [1] S. Chen, B. Liu, C. Feng *et al.*, "3D point cloud processing and learning for autonomous driving: Impacting map creation, localization, and perception," *IEEE Signal Processing Magazine*, vol. 38, no. 1, pp. 68–86, 2021. **1**
- [2] Q. Cheng, P. Sun, C. Yang *et al.*, "A morphing-based 3D point cloud reconstruction framework for medical image processing," *Computer Methods and Programs in Biomedicine*, vol. 193, p. 105495, 2020. **1**
- [3] S. Schwarz, M. Preda, V. Baroncini *et al.*, "Emerging MPEG standards for point cloud compression," *IEEE Journal on Emerging and Selected Topics in Circuits and Systems*, vol. 9, no. 1, pp. 133–148, 2019. **1**
- [4] A. Ak, E. Zerman, M. Quach *et al.*, "BASICS: Broad quality assessment of static point clouds in compression scenarios," *arXiv preprint arXiv:2302.04796*, 2023. **1**
- [5] B. Fei, W. Yang, W. Chen *et al.*, "Comprehensive review of deep learning-based 3d point cloud completion processing and analysis," *IEEE Transactions on Intelligent Transportation Systems*, vol. 23, no. 12, pp. 22 862–22 883, 2022. **1**
- [6] L. Zhou, G. Sun, Y. Li *et al.*, "Point cloud denoising review: from classical to deep learning-based approaches," *Graphical Models*, vol. 121, p. 101140, 2022. **1**
- [7] R. K. Mantiuk, A. Tomaszewska, and R. Mantiuk, "Comparison of four subjective methods for image quality assessment," *Computer Graphics Forum*, vol. 31, no. 8, pp. 2478–2491, 2012. **1**
- [8] X. Yang, F. Li, and H. Liu, "A survey of DNN methods for blind image quality assessment," *IEEE Access*, vol. 7, pp. 123 788–123 806, 2019. **1**
- [9] E. P. Simoncelli and B. A. Olshausen, "Natural image statistics and neural representation," *Annual Review of Neuroscience*, vol. 24, no. 1, pp. 1193–1216, 2001. **1**
- [10] G. Felsen and Y. Dan, "A natural approach to studying vision," *Nature Neuroscience*, vol. 8, no. 12, pp. 1643–1646, 2005. **1**
- [11] Y. Liu, Q. Yang, Y. Xu, and L. Yang, "Point cloud quality assessment: Dataset construction and learning-based no-reference metric," *ACM Transactions on Multimedia Computing Communications and Applications*, vol. 19, no. 2s, pp. 1–26, 2023. **2, 3, 12, 13**
- [12] Q. Yang, H. Chen, Z. Ma *et al.*, "Predicting the perceptual quality of point cloud: A 3d-to-2d projection-based exploration," *IEEE Transactions on Multimedia*, vol. 23, pp. 3877–3891, 2021. **2, 3, 8, 12**
- [13] Q. Yang, J. Jung, T. Deschamps *et al.*, "TMD: A database for dynamic color mesh subjective and objective quality explorations," in *ACM International Conference on Multimedia*, 2023, pp. 1–1. **2**
- [14] E. Alexiou, N. Yang, and T. Ebrahimi, "PointXR: A toolbox for visualization and subjective evaluation of point clouds in virtual reality," in *International Conference on Quality of Multimedia Experience*, 2020, pp. 1–6. **2**
- [15] A. Javaheri, C. Brites, F. Pereira, and J. Ascenso, "Point cloud rendering after coding: Impacts on subjective and objective quality," *IEEE Transactions on Multimedia*, vol. 23, pp. 4049–4064, 2021. **2**
- [16] S. Perry, H. P. Cong, L. A. da Silva Cruz *et al.*, "Quality evaluation of static point clouds encoded using MPEG codecs," in *IEEE International Conference on Image Processing*, 2020, pp. 3428–3432. **2**
- [17] E. Alexiou, I. Viola, T. M. Borges *et al.*, "A comprehensive study of the rate-distortion performance in MPEG point cloud compression," *APSIPA Transactions on Signal and Information Processing*, vol. 8, p. e27, 2019. **2**
- [18] H. Su, Z. Duanmu, W. Liu *et al.*, "Perceptual quality assessment of 3D point clouds," in *IEEE International Conference on Image Processing*, 2019, pp. 3182–3186. **2, 12, 13**
- [19] Q. Liu, H. Su, Z. Duanmu *et al.*, "Perceptual quality assessment of colored 3D point clouds," *IEEE Transactions on Visualization and Computer Graphics*, pp. 1–1, 2022. **2, 12, 13**
- [20] G. Kulkarni, V. Premraj, V. Ordonez *et al.*, "BabyTalk: Understanding and generating simple image descriptions," *IEEE Transactions on Pattern Analysis and Machine Intelligence*, vol. 35, no. 12, pp. 2891–2903, 2013. **2**
- [21] C. D. Aitkin, "Discretization of continuous features by human learners," Ph.D. dissertation, Rutgers, The State University of New Jersey, 2009. **2**
- [22] ITU-R, "Methodology for the subjective assessment of the quality of television pictures," *ITU-R Recommendation BT.500-13*, 2012. **2, 4, 6, 8, 9**
- [23] P. Cignoni, C. Rocchini, and R. Scopigno, "Metro: measuring error on simplified surfaces," *Computer Graphics Forum*, vol. 17, no. 2, pp. 167–174, 1998. **3, 13**
- [24] D. Tian, H. Ochimizu, C. Feng *et al.*, "Evaluation metrics for point cloud compression," *ISO/IEC JTC m74008, Geneva, Switzerland*, 2017. **3**
- [25] MPEG, "MPEG reference software," <http://mpegx.int-ervy.fr/software/MPEG/PCC/TM/mpeg-pcc-dmetric>, 2022. **3, 13**
- [26] E. Alexiou and T. Ebrahimi, "Point cloud quality assessment metric based on angular similarity," in *IEEE International Conference on Multimedia and Expo*, 2018, pp. 1–6. **3**
- [27] A. Javaheri, C. Brites, F. Pereira, and J. Ascenso, "A generalized Hausdorff distance based quality metric for point cloud geometry," in *International Conference on Quality of Multimedia Experience*, 2020, pp. 1–6. **3**
- [28] G. Meynet, J. Digne, and G. Lavoué, "PC-MSDM: A quality metric for 3D point clouds," in *International Conference on Quality of Multimedia Experience*, 2019, pp. 1–3. **3**
- [29] G. Meynet, Y. Nehmé, J. Digne, and G. Lavoué, "PCQM: A full-reference quality metric for colored 3d point clouds," in *International Conference on Quality of Multimedia Experience*, 2020, pp. 1–6. **3, 13**
- [30] I. Viola, S. Subramanyam, and P. Cesar, "A color-based objective quality metric for point cloud contents," in *International Conference on Quality of Multimedia Experience*, 2020, pp. 1–6. **3**
- [31] E. Alexiou and T. Ebrahimi, "Towards a point cloud structural similarity metric," in *IEEE International Conference on Multimedia and Expo Workshops*, 2020, pp. 1–6. **3**
- [32] Z. Wang, A. C. Bovik, H. R. Sheikh, and E. P. Simoncelli, "Image quality assessment: from error visibility to structural similarity," *IEEE Transactions on Image Processing*, vol. 13, no. 4, pp. 600–612, 2004. **3**
- [33] Q. Yang, Z. Ma, Y. Xu *et al.*, "Inferring point cloud quality via graph similarity," *IEEE Transactions on Pattern Analysis and Machine Intelligence*, vol. 44, no. 6, pp. 3015–3029, 2022. **3, 13**
- [34] Y. Zhang, Q. Yang, and Y. Xu, "MS-GraphSIM: Inferring point cloud quality via multiscale graph similarity," in *ACM International Conference on Multimedia*, 2021, p. 1230–1238. **3, 7**
- [35] A. Javaheri, C. Brites, F. Pereira, and J. Ascenso, "A point-to-distribution joint geometry and color metric for point cloud quality assessment," in *IEEE International Workshop on Multimedia Signal Processing*, 2021, pp. 1–6. **3**
- [36] E. M. Torlig, E. Alexiou, T. A. Fonseca *et al.*, "A novel methodology for quality assessment of voxelized point clouds," *Applications of Digital Image Processing XLI*, vol. 10752, p. 107520I, 2018. **3**
- [37] A. Javaheri, C. Brites, F. Pereira, and J. Ascenso, "Joint geometry and color projection-based point cloud quality metric," *IEEE Access*, vol. 10, pp. 90 481–90 497, 2022. **3**
- [38] I. Viola and P. Cesar, "A reduced reference metric for visual quality evaluation of point cloud contents," *IEEE Signal Processing Letters*, vol. 27, pp. 1660–1664, 2020. **3**
- [39] Q. Liu, H. Yuan, R. Hamzaoui *et al.*, "Reduced reference perceptual quality model with application to rate control for video-based point cloud compression," *IEEE Transactions on Image Processing*, vol. 30, pp. 6623–6636, 2021. **3**
- [40] Y. Liu, Q. Yang, and Y. Xu, "Reduced reference quality assessment for point cloud compression," in *IEEE International Conference on Visual Communications and Image Processing*, 2022, pp. 1–5. **3**
- [41] W. Tao, G. Jiang, Z. Jiang, and M. Yu, "Point cloud projection and multi-scale feature fusion network based blind quality assessment for colored point clouds," in *ACM International Conference on Multimedia*, 2021, p. 5266–5272. **3, 7**
- [42] Q. Liu, H. Yuan, H. Su *et al.*, "PQA-Net: Deep no reference point cloud quality assessment via multi-view projection," *IEEE Transactions on Circuits and Systems for Video Technology*, vol. 31, no. 12, pp. 4645–4660, 2021. **3, 10, 13**
- [43] Q. Yang, Y. Liu, S. Chen *et al.*, "No-reference point cloud quality assessment via domain adaptation," in *IEEE/CVF Conference on Computer Vision and Pattern Recognition*, 2022, pp. 21 179–21 188. **3, 8, 9, 13**
- [44] Y. Fan, Z. Zhang, W. Sun *et al.*, "A no-reference quality assessment metric for point cloud based on captured video sequences," in *IEEE International Workshop on Multimedia Signal Processing*, 2022, pp. 1–5. **3**
- [45] Z. Zhang, W. Sun, Y. Zhu *et al.*, "Treating point cloud as moving camera videos: A no-reference quality assessment metric," *arXiv preprint arXiv:2208.14085*, 2022. **3**



- [46] Z. Shan, Q. Yang, R. Ye *et al.*, "GPA-Net: No-reference point cloud quality assessment with multi-task graph convolutional network," *IEEE Transactions on Visualization and Computer Graphics*, pp. 1–1, 2023. [3](#), [13](#)
- [47] Z. Zhang, W. Sun, X. Min *et al.*, "MM-PCQA: Multi-modal learning for no-reference point cloud quality assessment," in *International Joint Conference on Artificial Intelligence*, 2023, pp. 1–1. [3](#), [13](#)
- [48] B. Schölkopf, R. Herbrich, and A. J. Smola, "A generalized representer theorem," in *International Conference on Computational Learning Theory*, 2001, pp. 416–426. [4](#)
- [49] N. J. Higham, "Computing a nearest symmetric positive semidefinite matrix," *Linear Algebra and its Applications*, vol. 103, pp. 103–118, 1988. [5](#)
- [50] T. Hospedales, A. Antoniou, P. Micaelli, and A. Storkey, "Meta-learning in neural networks: A survey," *IEEE Transactions on Pattern Analysis and Machine Intelligence*, vol. 44, no. 9, pp. 5149–5169, 2022. [6](#)
- [51] F. Sung, Y. Yang, L. Zhang *et al.*, "Learning to compare: Relation network for few-shot learning," in *IEEE/CVF Conference on Computer Vision and Pattern Recognition*, 2018, pp. 1199–1208. [6](#)
- [52] M. Quach, G. Valenzise, and F. Dufaux, "Folding-based compression of point cloud attributes," in *IEEE International Conference on Image Processing*, 2020, pp. 3309–3313. [7](#)
- [53] W. Zhang, K. Ma, J. Yan *et al.*, "Blind image quality assessment using a deep bilinear convolutional neural network," *IEEE Transactions on Circuits and Systems for Video Technology*, vol. 30, no. 1, pp. 36–47, 2020. [9](#)
- [54] M. Guo, J. Cai, Z. Liu *et al.*, "PCT: Point cloud transformer," *Computational Visual Media*, vol. 7, no. 2, p. 187–199, 2021. [9](#)
- [55] A. Vaswani, N. Shazeer, N. Parmar *et al.*, "Attention is all you need," in *Advances in Neural Information Processing Systems*, vol. 30, 2017. [9](#), [10](#)
- [56] T. Chen, S. Kornblith, M. Norouzi, and G. Hinton, "A simple framework for contrastive learning of visual representations," in *International Conference on Machine Learning*, vol. 119, 2020, pp. 1597–1607. [10](#)
- [57] M. Blondel, O. Teboul, Q. Berthet, and J. Djolonga, "Fast differentiable sorting and ranking," in *International Conference on Machine Learning*, vol. 119, 2020, pp. 950–959. [10](#)
- [58] E. Alexiou and T. Ebrahimi, "Exploiting user interactivity in quality assessment of point cloud imaging," in *International Conference on Quality of Multimedia Experience*, 2019, pp. 1–6. [13](#)
- [59] R. Mekuria, Z. Li, C. Tulvan, and P. Chou, "Evaluation criteria for point cloud compression," *ISO/IEC MPEG w16332, Geneva, Switzerland*, 2016. [13](#)
- [60] Q. Yang, Y. Zhang, S. Chen *et al.*, "MPED: Quantifying point cloud distortion based on multiscale potential energy discrepancy," *IEEE Transactions on Pattern Analysis and Machine Intelligence*, vol. 45, no. 5, pp. 6037–6054, 2023. [13](#)